Artificial plasma formed by connected metallic wires at infrared frequencies

Mário G. Silveirinha*
Departamento de Engenharia Electrotécnica, Instituto de Telecomunicações, Universidade de Coimbra, Pólo II, 3030 Coimbra, Portugal

(Received 29 August 2008; revised manuscript received 21 November 2008; published 22 January 2009)

In this work, we investigate the influence of the plasmonic properties of metal and the effect of metal loss in the effective-medium properties of wire media formed by an array of connected rods at infrared frequencies. Using homogenization techniques, it is demonstrated that the plasmonic properties of metals may enable the design of artificial plasmas that mimic more closely the behavior of a continuous isotropic medium with negative permittivity. It is shown that when the plasmonic properties of the metal are dominant, the electrical length of the unit cell may be a very small fraction of the operating wavelength near the plasma frequency of the wire medium and that the spatial dispersion effects may be relatively weak. In addition, we investigate the possibility operating the artificial plasma in the regime $\mathrm{Re}\{\varepsilon\}=-1$ to obtain a superlensing effect at infrared frequencies analogous to that characteristic of the silver lens.

DOI: 10.1103/PhysRevB.79.035118 PACS number(s): 42.70.Qs, 78.20.Ci, 41.20.Jb

I. INTRODUCTION

Materials with the real part of the permittivity negative or near zero have raised significant interest in recent works. These materials may play an important role in applications such as near-field imaging,[1–3] realization of double negative media,[4] tunneling through narrow channels,[5] and novel nanocircuits.[6] Even though at some very specific infrared and optical frequencies materials with the desired properties may be readily available in nature (e.g., noble metals at optical or UV frequencies), in general these materials need to be assembled in the form of "metamaterials:" composite structures formed by dielectric or metallic inclusions whose geometry and material parameters determine the macroscopic electromagnetic response. A typical configuration for artificial media with negative permittivity consists of a periodic lattice formed by thin metallic wires. This structure has been known at least since the 1950s (Refs. 7 and 8) and has been rediscovered and brought into a new light in Ref. 9. It was revisited in several more recent works,[10–15] which have emphasized the role of spatial dispersion in wire metamaterials and how it may affect and modify the material response in comparison to a local material. Even though such wire metamaterials have been successfully used in several problems, to our knowledge up to now there is no conclusive evidence that such artificial plasmas may support localized modes that truly mimic the properties of "surface plasmons" in metals. These localized modes are arguably the most interesting feature of materials with negative permittivity since they may enable the realization of extremely compact waveguides and resonators and phenomena such as superlensing[1,2] and artificial magnetism.[16] Indeed, it was shown in Ref. 13 that for a medium formed by perfectly electric conducting (PEC) wires the guided mode at an interface between the artificial plasma and air is very weakly bounded to the interface in the regime $\mathrm{Re}\{\varepsilon\}=-1$, very different from what happens in a bulk metal. The two main reasons for this property are (i) the granularity of the structured material and (ii) spatial dispersion effects.

The granularity effect stems from the relatively large electrical length of the lattice constant of the wire medium at the plasma frequency, usually something like $a\approx 0.2\lambda_0$. Typically, homogenization is valid only if $\omega a/c \ll \pi$ and $ka \ll \pi$, where ω is the radian frequency, c is the speed of light, and k is the wave number in the material. The surface plasmons at an interface between a metal and a dielectric may be associated with large values of k: $kc/\omega \gg 1$. It is clear that the conditions $kc/\omega \gg 1$ and $ka \ll \pi$ cannot be simultaneously verified if the lattice constant is large as $a\approx 0.2\lambda_0$ at the frequency of interest, which justifies the results in Ref. 13. Moreover, as long as the metal conductivity is very large (e.g., at microwaves), the relatively large values of a/λ_0 at the plasma frequency seem to be the characteristic of wire media and set a fundamental limitation in the properties of the structured material.

The second reason for the very different behavior of surface modes in artificial plasmas as compared to bulk metals is spatial dispersion. As proven in Ref. 12, the main effect of spatial dispersion in systems formed by connected metallic wires is that they support a dispersive longitudinal mode. Indeed, very differently from a local continuous material for which a longitudinal mode is forbidden with the exception of the plasma frequency, in a wire metamaterial the longitudinal mode may be supported in a relatively wide range of frequencies above the plasma frequency.[12,13] As a consequence, the longitudinal mode may be excited and significantly affect the propagation characteristics of surface modes and the electromagnetic response of the structured material. For example, it is known that spatial dispersion effects may influence the quality of near-field imaging.[17] In a recent work,[15] it was shown that spatial dispersion effects in wire media may be tamed either by increasing the capacitance of the wires or by coating the wires with a magnetic material.

In this work, we show a completely different possibility to drastically reduce both the effect of spatial dispersion and the size of the lattice constant a at the plasma frequency. Using homogenization techniques, we demonstrate that in the infrared domain the constraints on the wire medium properties are much less strict than in the microwave domain and that it may be possible to take advantage of the plasmonic properties of noble metals to obtain a structured material that mimics more closely the properties of a local isotropic plasma.

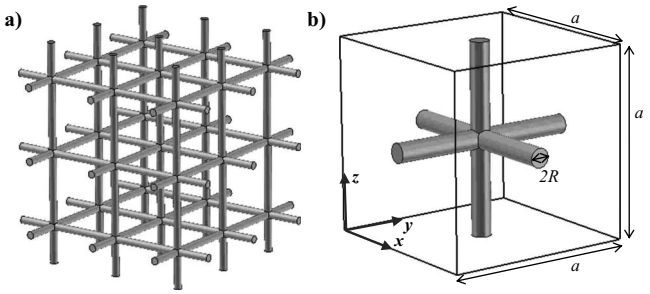

FIG. 1. Geometry of a triple array of connected metallic wires: (a) Sample of the periodic material. (b) Unit cell. The radius of the rods is R and the lattice constant is a.

The geometry of the wire medium considered here is analogous to that of our previous work[12] and is reported in Fig. 1. However, unlike previous works related to this inclusion topology,[12–15] here we fully take into account the plasmonic properties and the metallic loss in the wires. These effects were also considered in Refs. 18 and 19, however such studies dealt exclusively with arrays of parallel rods. It is important to note that it is impossible to predict the propagation properties of the longitudinal mode supported by the structure of Fig. 1 from the results of these previous studies. Here, we derive the dielectric function of the artificial plasma depicted in Fig. 1, fully taking into account the plasmonic and loss effects in the metallic rods, and discuss the possibility of using such material to obtain near-field imaging.

This paper is organized as follows. In Sec. II, we briefly review the homogenization approach introduced in Ref. 20. In Sec. III, before considering the more demanding geometry of Fig. 1, we use the homogenization technique to characterize the dielectric function of an array of parallel wires. The advantage of making this small detour is that it permits to illustrate the application of the homogenization method to a very simple system. In Sec. IV, we tackle the more difficult homogenization problem of connected wires (Fig. 1) and calculate its dielectric function using analytical techniques. In Sec. V, the plane-wave solutions supported by the bulk artificial plasma are characterized. It is shown that the waves can be classified into transverse and longitudinal modes. The influence of plasmonic properties and loss in the metallic wires are thoroughly discussed. In Sec. VI, the homogenization model is applied to calculate the transfer function of a thin material slab in the regime $\mathrm{Re}\{\varepsilon_t\}=-1$, and the results are validated with full wave simulations. The possibility of near-field imaging is discussed. In Sec. VII, we study the frequency response of the artificial material slab and in particular investigate the existence of oscillations in the transmission characteristic above the plasma frequency. Finally, in Sec. VIII the conclusion is drawn. In this work, it is assumed that the electromagnetic fields have a time variation in the form $e^{j\omega t}$, where $j=\sqrt{-1}$.

II. HOMOGENIZATION METHOD

To calculate the dielectric function of the wire medium we will use the homogenization technique introduced in our previous works.[20–22] The method in Ref. 20 is completely general and allows us to homogenize a structured material formed by arbitrarily shaped dielectric or metallic inclusions using a nonlocal dielectric function of the form $\bar{\bar{\varepsilon}}=\bar{\bar{\varepsilon}}(\omega,\mathbf{k})$. Notice that the effective dielectric function may depend on the wave vector $\mathbf{k}=(k_x,k_y,k_z)$, as a consequence of possible spatial dispersion effects.[23,24] Simply put, the idea to extract the effective parameters is to excite the metamaterial with a suitable periodic source distribution and then to calculate $\bar{\bar{\varepsilon}}(\omega,\mathbf{k})$ from the average (macroscopic) electromagnetic fields and the generalized polarization vector. For further details the reader is referred to Ref. 20.

Here, we will consider the particular case in which the structured material is formed by inclusions that can be described to some approximation by an impedance boundary condition such that

$$\mathbf{E}_{\tan}=Z_s\mathbf{J}_s \quad \text{at} \quad \partial D, \tag{1}$$

where ∂D is the boundary surface of the inclusion, $\mathbf{E}_{\tan}$ is the tangential electric field, $\mathbf{J}_s=\hat{\boldsymbol{\nu}}\times\mathbf{H}$ is the surface density of current, $\hat{\boldsymbol{\nu}}$ is the unit normal vector oriented to the exterior of the inclusion, and Z_s is the surface impedance. For example, a perfectly conducting inclusion can be described by the surface impedance $Z_s=0$. As will be discussed below, thin metallic wires may be accurately characterized using a surface impedance model.

Following the same steps as in Ref. 20 and solving the homogenization problem using the method of moments (MoM), it may be proven that the effective dielectric function of a periodic material formed by arbitrarily shaped inclusions standing in air and characterized by the surface impedance Z_s is given by

$$\frac{\bar{\bar{\varepsilon}}}{\varepsilon_0}(\omega,\mathbf{k})=\bar{\bar{\mathbf{I}}}+\frac{1}{V_{\text{cell}}}\sum_{m,n}\chi^{m,n}\left(\int_{\partial D}\mathbf{w}_{m,\mathbf{k}}(\mathbf{r})e^{+j\mathbf{k}\cdot\mathbf{r}}ds\right)\otimes\left(\int_{\partial D}\mathbf{w}_{n,-\mathbf{k}}(\mathbf{r})e^{-j\mathbf{k}\cdot\mathbf{r}}ds\right), \tag{2a}$$

$$\chi_{m,n}=\int_{\partial D}\int_{\partial D}[\nabla_s\cdot\mathbf{w}_{m,-\mathbf{k}}(\mathbf{r})\nabla_s'\cdot\mathbf{w}_{n,\mathbf{k}}(\mathbf{r}')-(\omega/c)^2\mathbf{w}_{m,-\mathbf{k}}(\mathbf{r})\cdot\mathbf{w}_{n,\mathbf{k}}(\mathbf{r}')]\Phi_{p0}(\mathbf{r}|\mathbf{r}';\omega,\mathbf{k})dsds'+j\omega\varepsilon_0Z_s\int_{\partial D}\mathbf{w}_{m,-\mathbf{k}}(\mathbf{r})\cdot\mathbf{w}_{n,\mathbf{k}}(\mathbf{r})ds, \tag{2b}$$

where $\bar{\bar{\mathbf{I}}}$ is the identity dyadic, V_{cell} is the volume of the unit cell, $\mathbf{w}_1,\mathbf{w}_2,\ldots$ form a complete set of tangential vector fields over ∂D, and Φ_{p0} is Green's function introduced in Ref. 20. In the above, $\nabla_s\cdot$ stands for the surface divergence of a tangential vector field and the matrix $[\chi^{m,n}]$ is the inverse of $[\chi_{m,n}]$. As explained in Ref. 20, the expansion functions must have the Floquet-Bloch property when the inclusions intersect the boundaries of the unit cell. Due to this reason, in general the expansion functions depend explicitly on the wave vector $\mathbf{k}$, i.e., $\mathbf{w}_n=\mathbf{w}_{n,\mathbf{k}}(\mathbf{r})$.

The interaction of electromagnetic waves with a thin metallic wire characterized by the relative complex permittivity ε_m with $\mathrm{Re}\{\varepsilon_m\}\ll 0$ may be described to a good approxima-

tion using a surface impedance model. The equivalent surface impedance is given by

$$Z_s = \frac{2}{j\omega\varepsilon_0(\varepsilon_m - 1)R}, \tag{3}$$

where R is the radius of the wire. The above formula is obtained as follows. The volumetric density of current induced in a metallic wire is given by $\mathbf{J}_d = j\omega\varepsilon_0(\varepsilon_m - 1)\mathbf{E}$. Assuming that $\mathbf{J}_d$ is approximately constant in the wire cross section, the total current that flows along the wire is $I = j\omega\varepsilon_0(\varepsilon_m - 1)E_z\pi R^2$, where E_z is the electric field component along the wire axis (let us say the z axis). In case the same metallic wire can be described to some approximation by surface impedance model (1), the current is given by $I = 2\pi R E_z / Z_s$. By comparing the two formulas for the current, it is readily found that the surface impedance must verify Eq. (3). The surface impedance model is expected to be accurate as long as the wires are very thin ($R \ll \lambda_0$) and $\mathrm{Re}\{\varepsilon_m\} \ll 0$ so that it makes no significant difference to assume that the current is uniformly distributed along the cross section or that it flows exclusively on the surface of the wire. The condition $\mathrm{Re}\{\varepsilon_m\} \ll 0$ is verified by noble metals at infrared frequencies and below. Substituting Eq. (3) into Eq. (2b), it is found that $\chi_{m,n}$ can be written as

$$\chi_{m,n} = \int_{\partial D}\int_{\partial D} [\nabla_s \cdot \mathbf{w}_{m,-\mathbf{k}}(\mathbf{r})\nabla'_s \cdot \mathbf{w}_{n,\mathbf{k}}(\mathbf{r}') - (\omega/c)^2 \mathbf{w}_{m,-\mathbf{k}}(\mathbf{r}) \cdot \mathbf{w}_{n,\mathbf{k}}(\mathbf{r}')]\Phi_{p0}(\mathbf{r}|\mathbf{r}';\omega,\mathbf{k})dsds' + \frac{2}{(\varepsilon_m - 1)R}\int_{\partial D} \mathbf{w}_{m,-\mathbf{k}}(\mathbf{r}) \cdot \mathbf{w}_{n,\mathbf{k}}(\mathbf{r})ds. \tag{4}$$

III. DIELECTRIC FUNCTION OF AN ARRAY OF PARALLEL WIRES

Before considering the homogenization of the structure formed by connected wires (Fig. 1), it is useful to consider the simpler case in which all the wires are parallel and oriented along the z axis. This will enable us to illustrate the homogenization methods that will be used to characterize the connected wire medium, without having to lose too much time with lengthy mathematical details. It is assumed that the array of parallel wires is arranged in a square lattice with lattice constant a, and that the electromagnetic response of a metallic wire can be modeled by surface impedance model (3).

The effective dielectric function $\bar{\bar{\varepsilon}}$ of the wire medium can be rigorously calculated by considering a complete set of expansion functions $\mathbf{w}_{n,\mathbf{k}}$. However, our objective here is to derive an approximate formula for the dielectric function valid in the long-wavelength limit. To begin with, it is convenient to remember that $\mathbf{w}_{n,\mathbf{k}}$ are the expansion functions for the density of current induced on the wires when the electromagnetic crystal is excited by an external source with the Floquet-Bloch property.[20] Thus, the induced current, and consequently the expansion functions, are also Floquet-$\mathbf{k}$ periodic. Since the wires are very thin, $R \ll a$, it can be assumed that the equivalent surface current is uniform in the cross section of the wires and flows exclusively along the axes of the rods. Thus, since the structure is invariant to translations along the z direction, it follows that one single expansion function is sufficient to describe the behavior of the induced density of current,

$$\mathbf{w}_{1,\mathbf{k}}(\mathbf{r}) = \frac{e^{-j\mathbf{k}\cdot\mathbf{r}}}{2\pi R}\hat{\mathbf{u}}_z, \tag{5}$$

where $\hat{\mathbf{u}}_z$ represents a unit vector directed along the z direction. Substituting this formula in Eq. (2a), it is readily found that

$$\frac{\bar{\bar{\varepsilon}}}{\varepsilon_0}(\omega,\mathbf{k}) = \bar{\bar{\mathbf{I}}} + \frac{1}{a}\frac{1}{\chi_{11}(\omega,\mathbf{k})}\hat{\mathbf{u}}_z\hat{\mathbf{u}}_z, \tag{6}$$

where $\hat{\mathbf{u}}_z\hat{\mathbf{u}}_z \equiv \hat{\mathbf{u}}_z \otimes \hat{\mathbf{u}}_z$ represents the dyadic (tensor) product of the two vectors, $\chi_{11}(\omega,\mathbf{k})$ is calculated using Eq. (4), and is given by

$$\chi_{11} = \left(k_z^2 - \frac{\omega^2}{c^2}\right)\frac{1}{(2\pi R)^2}\int_{\partial D}\int_{\partial D} e^{j\mathbf{k}\cdot(\mathbf{r}-\mathbf{r}')}\Phi_{p0}(\mathbf{r}|\mathbf{r}';\omega,\mathbf{k})dsds' + \frac{1}{(\varepsilon_m - 1)}\frac{a}{\pi R^2}, \tag{7}$$

and $\partial D = \{(x,y,z): x^2 + y^2 < R^2 \text{ and } |z| < a/2\}$ represents the surface of the plasmonic wire in the unit cell. Hence, the dielectric function can be written as

$$\frac{\bar{\bar{\varepsilon}}}{\varepsilon_0}(\omega,\mathbf{k}) = \bar{\bar{\mathbf{I}}} + \frac{1}{\frac{1}{(\varepsilon_m - 1)}\frac{1}{f_V} + \frac{1}{\beta_p^2}\left(k_z^2 - \frac{\omega^2}{c^2}\right)}\hat{\mathbf{u}}_z\hat{\mathbf{u}}_z, \tag{8}$$

where $f_V = \pi R^2/a^2$ is the volume fraction of the wires, and β_p is defined by

$$\frac{1}{\beta_p^2} = \frac{a}{(2\pi R)^2}\int_{\partial D}\int_{\partial D} e^{j\mathbf{k}.(\mathbf{r}-\mathbf{r}')}\Phi_{p0}(\mathbf{r}|\mathbf{r}';\omega,\mathbf{k})dsds'. \tag{9}$$

Green's function Φ_{p0} has the following plane-wave expansion:[20]

$$\Phi_{p0} = \frac{1}{V_{\text{cell}}}\sum_{\mathbf{J}\neq 0}\frac{e^{-j\mathbf{k}_\mathbf{J}\cdot(\mathbf{r}-\mathbf{r}')}}{\mathbf{k}_\mathbf{J}\cdot\mathbf{k}_\mathbf{J} - (\omega/c)^2} \approx \frac{e^{-j\mathbf{k}\cdot(\mathbf{r}-\mathbf{r}')}}{V_{\text{cell}}}\sum_{\mathbf{J}\neq 0}\frac{e^{-j\mathbf{k}_\mathbf{J}^0\cdot(\mathbf{r}-\mathbf{r}')}}{\mathbf{k}_\mathbf{J}^0\cdot\mathbf{k}_\mathbf{J}^0}, \tag{10}$$

where $\mathbf{J} = (j_1, j_2, j_3)$ is a generic triple index of integers, $\mathbf{k}_\mathbf{J} = \mathbf{k} + \mathbf{k}_\mathbf{J}^0$, and $\mathbf{k}_\mathbf{J}^0 = (j_1, j_2, j_3)2\pi/a$ is a reciprocal-lattice vector. The second identity is valid in the long-wavelength limit, $\omega/c \ll \pi/a$ and $|\mathbf{k}| \ll \pi/a$, and is assumed in the following. Substituting Eq. (10) into Eq. (9), and performing the integrations analytically it may be shown that

$$\frac{1}{\beta_p^2} = \left(\frac{a}{2\pi}\right)^2 \sum_{(m,n)\neq(0,0)} \frac{\left[J_0\left(\frac{2\pi R}{a}\sqrt{m^2+n^2}\right)\right]^2}{m^2+n^2}, \tag{11}$$

where m and n are generic integers, and J_0 is the Bessel function of first kind and order zero. Following the results in Ref. 12, β_p can be identified with the plasma wave number

for an array of parallel PEC wires. It may be verified that the above formula is in very good agreement with the result obtained in Ref. 11

$$(\beta_p a)^2 = \frac{2\pi}{\ln\left(\frac{a}{2\pi R}\right) + 0.5275}. \quad (12)$$

Formula (8) gives the dielectric function of the array of parallel plasmonic wires, and is completely consistent with the formula derived in our earlier work[18] using a more complicated local-field approach (see also Ref. 19). In fact, it is remarkable how using the general homogenization theory proposed in Ref. 20, it was possible to characterize the effective properties of the wire medium in a very straightforward manner. Moreover, the fact that we obtained the exact same result as in Ref. 18 supports that surface impedance model (3) can be used to accurately characterize the plasmonic properties of the metallic wires.

As described in Ref. 18, the dielectric function of the composite material depends strongly on the wave vector component k_z, and consequently it is characterized by strong spatial dispersion. For a detailed discussion of the electrodynamics of such wire medium the reader is referred to Ref. 18.

IV. DIELECTRIC FUNCTION OF THE CONNECTED WIRE MEDIUM

The dielectric function of the connected medium can be calculated following a strategy similar to that used in Sec. III, adapting also some ideas of our previous work.[12] It is clear that the homogenization of the connected wire medium requires additional expansion functions for the electric current because in the geometry of Fig. 1, the wires are directed along the x, y, and z directions. It is convenient to decompose the surface of the wires contained in the unit cell as follows:

$$\partial D = \bigcup_i \partial D_i, \quad (13)$$

where ∂D_i represents the surface of the wire directed along the i direction, being $i=1,2,3=x,y,z$. Using the same arguments as in Sec. III, the expansion functions are now taken equal to $\mathbf{w}_{n,\mathbf{k}} = \mathbf{w}^{\mathrm{I}}_{n,\mathbf{k}}$, with $n=1,2,3$, where $\mathbf{w}^{\mathrm{I}}_{n,\mathbf{k}}$ are such that

$$\mathbf{w}^{\mathrm{I}}_{n,\mathbf{k}}|_{\partial D_i} = \frac{e^{-j\mathbf{k}\cdot\mathbf{r}}}{2\pi R}\hat{\mathbf{u}}_n \delta_{n,i}, \quad (14)$$

where $\delta_{n,i}$ represents the Kronecker's symbol: $\delta_{n,i}=1$ if $n=i$, and $\delta_{n,i}=0$ otherwise. Hence, the expansion function $\mathbf{w}^{\mathrm{I}}_{n,\mathbf{k}}$ models a current that flows exclusively along the metallic wire directed along the n direction ($n=1,2,3=x,y,z$). As discussed in Ref. 12, the set of expansion functions $\mathbf{w}^{\mathrm{I}}_{n,\mathbf{k}}$ is insufficient to characterize the current that flows along the wires. Indeed, since the wires are connected, the electric current along a given wire may be discontinuous at the junction because part of the current may be redirected through another orthogonal wire. In order to take into account the mutual coupling between orthogonal wires it is necessary to consider two additional expansion functions:[12] $\mathbf{w}^{\mathrm{II}}_{n',\mathbf{k}}$ with $n'=1,2$. The expansion functions $\mathbf{w}^{\mathrm{II}}_{n',\mathbf{k}}$ are such that

$$\mathbf{w}^{\mathrm{II}}_{n',\mathbf{k}}|_{\partial D_i} = \frac{e^{-j\mathbf{k}\cdot\mathbf{r}}}{2\pi R} s(x_i)\boldsymbol{\alpha}_{n'}\cdot\hat{\mathbf{u}}_i\hat{\mathbf{u}}_i \quad (i=1,2,3), \quad (15)$$

where $\boldsymbol{\alpha}_{n'}$ ($n'=1,2$) is a constant vector defined below, $x_i = \mathbf{r}\cdot\hat{\mathbf{u}}_i$ is the space coordinate along the i direction, and $s(x)$ is the "saw" function introduced in Ref. 12. It is defined by

$$s(x) = \frac{1}{2} - \frac{x}{a}, \quad 0 < x < a, \quad (16)$$

and it is periodically extended to the real line with period a. In particular, the "saw" function is discontinuous at points of the form $x=ma$ with $m=0,\pm 1,\ldots$, with a step discontinuity equal to $[s]=s(0^+)-s(0^-)=1$. Hence, it is clear that the expansion functions $\mathbf{w}^{\mathrm{II}}_{n',\mathbf{k}}$ are also discontinuous at the junction point in the unit cell ($\mathbf{r}=0$). As discussed in Ref. 12, since there is no charge stored at the wire junction, the expansion functions need to ensure that the total current that arrives at the junction is equal to the total current that emerges from the junction (i.e., Kirchoff's current law). It is simple to verify that this condition is obeyed provided $\boldsymbol{\alpha}_{n'}$ is such that

$$\boldsymbol{\alpha}_{n'}\cdot\boldsymbol{\alpha}_3 = 0, \quad n'=1,2, \quad \text{where } \boldsymbol{\alpha}_3 = \frac{1}{\sqrt{3}}(1,1,1). \quad (17)$$

For convenience, it is supposed that $\boldsymbol{\alpha}_1$ and $\boldsymbol{\alpha}_2$ are orthogonal and have unity norm. Thus, they verify

$$\boldsymbol{\alpha}_n\cdot\boldsymbol{\alpha}_m = \delta_{n,m}, \quad n,m=1,2,3, \quad (18)$$

where $\boldsymbol{\alpha}_3$ is defined as in Eq. (17). We will not assume any explicit form for $\boldsymbol{\alpha}_1$ and $\boldsymbol{\alpha}_2$ since the dielectric function of the wire medium will be independent of the specific choice of $\boldsymbol{\alpha}_1$ and $\boldsymbol{\alpha}_2$.

We will calculate the dielectric function of the connected wire medium, assuming that the five expansion functions $\mathbf{w}^{\mathrm{I}}_{n,\mathbf{k}}$ ($n=1,2,3$) and $\mathbf{w}^{\mathrm{II}}_{n',\mathbf{k}}$ ($n'=1,2$) are sufficient to model the density of current induced in the metallic wires. Using Eq. (2) it is simple to verify that within this hypothesis the dielectric function is given by

$$\frac{\bar{\bar{\varepsilon}}}{\varepsilon_0}(\omega,\mathbf{k}) = \bar{\bar{\mathbf{I}}} + \frac{1}{a}\sum_{m,n=1}^{3}(\chi^{\mathrm{I,I}})_{m,n}\hat{\mathbf{u}}_m\hat{\mathbf{u}}_n, \quad (19)$$

where $(\chi^{\mathrm{I,I}})_{m,n}$ represents the (m,n) element of the 3×3 matrix $\chi^{\mathrm{I,I}}$ defined next. Let $\boldsymbol{\chi}$ be the 5×5 matrix such that

$$\boldsymbol{\chi} = \begin{bmatrix} \chi_{\mathrm{I,I}} & \chi_{\mathrm{I,II}} \\ \chi_{\mathrm{II,I}} & \chi_{\mathrm{II,II}} \end{bmatrix}, \quad (20)$$

where the submatrices $\chi_{\mathrm{I,I}}$, $\chi_{\mathrm{I,II}}$, $\chi_{\mathrm{II,I}}$, and $\chi_{\mathrm{II,II}}$ have dimensions 3×3, 3×2, 2×3, and 2×2, respectively, and are defined consistently with Eq. (4). For example, a generic element of the matrix $\chi_{\mathrm{I,II}}$ is given by

$$(\chi_{\mathrm{I,II}})_{m,n'} = \int_{\partial D}\int_{\partial D} [\nabla_s \cdot \mathbf{w}^{\mathrm{I}}_{m,-\mathbf{k}}(\mathbf{r})\nabla'_s \cdot \mathbf{w}^{\mathrm{II}}_{n',\mathbf{k}}(\mathbf{r}') - (\omega/c)^2 \mathbf{w}^{\mathrm{I}}_{m,-\mathbf{k}}(\mathbf{r}) \cdot \mathbf{w}^{\mathrm{II}}_{n',\mathbf{k}}(\mathbf{r}')]\Phi_{p0}(\mathbf{r}|\mathbf{r}';\omega,\mathbf{k})dsds' + \frac{2}{(\varepsilon_m - 1)R}\int_{\partial D} \mathbf{w}^{\mathrm{I}}_{m,-\mathbf{k}}(\mathbf{r}) \cdot \mathbf{w}^{\mathrm{II}}_{n',\mathbf{k}}(\mathbf{r})ds. \quad (21)$$

The inverse of $\boldsymbol{\chi}$ is decomposed as follows:

$$\boldsymbol{\chi}^{-1} = \begin{bmatrix} \chi^{\mathrm{I,I}} & \chi^{\mathrm{I,II}} \\ \chi^{\mathrm{II,I}} & \chi^{\mathrm{II,II}} \end{bmatrix}, \quad (22)$$

where the submatrices $\chi^{\mathrm{I,I}}$, $\chi^{\mathrm{I,II}}$, $\chi^{\mathrm{II,I}}$, and $\chi^{\mathrm{II,II}}$ have dimensions 3×3, 3×2, 2×3, and 2×2, respectively. Thus, the submatrix $\chi^{\mathrm{I,I}}$ which determines the dielectric function of the connected wire medium in Eq. (19) is such that

$$\chi^{\mathrm{I,I}} = (\chi_{\mathrm{I,I}} - \chi_{\mathrm{I,II}} \cdot \chi^{-1}_{\mathrm{II,II}} \cdot \chi_{\mathrm{II,I}})^{-1}. \quad (23)$$

Hence, it is clear that Eq. (19) implies that

$$\frac{\bar{\bar{\varepsilon}}}{\varepsilon_0}(\omega,\mathbf{k}) = \bar{\bar{\mathbf{I}}} + \frac{1}{a}(\chi_{\mathrm{I,I}} - \chi_{\mathrm{I,II}} \cdot \chi^{-1}_{\mathrm{II,II}} \cdot \chi_{\mathrm{II,I}})^{-1}. \quad (24)$$

Therefore, the dielectric function of the material can be completely characterized by the submatrices $\chi_{\mathrm{I,I}}$, $\chi_{\mathrm{I,II}}$, $\chi_{\mathrm{II,I}}$, and $\chi_{\mathrm{II,II}}$. The evaluation of these matrices is rather tedious, but the calculations are rather similar to the ones of our previous paper,[12] and thus we will only present the final result. Detailed calculations show that

$$(\chi_{\mathrm{I,I}})_{m,n} = \frac{1}{a}\frac{1}{\beta_1^2}\left(k_m k_n - \frac{\omega^2}{c^2}\delta_{m,n}\right) + \frac{1}{a}\left[\frac{1}{\varepsilon_m - 1}\frac{1}{f_V} + \left(\frac{1}{\beta_p^2} - \frac{1}{\beta_1^2}\right)\left(k_m^2 - \frac{\omega^2}{c^2}\right)\right]\delta_{m,n}, \quad (25a)$$

$$(\chi_{\mathrm{II,II}})_{m',n'} = \left[\frac{1}{a}\frac{1}{\varepsilon_m - 1}\frac{1}{f_V}\frac{1}{12} + \frac{1}{a^3}\left(\frac{1}{\beta_p^2} - \frac{1}{\beta_1^2}\right)\right]\delta_{m',n'} + \frac{1}{a\beta_2^2}\boldsymbol{\alpha}_{m'} \cdot \sum_{l=1}^{3}\left(k_l^2 - \frac{\omega^2}{c^2}\right)\hat{\mathbf{u}}_l\hat{\mathbf{u}}_l \cdot \boldsymbol{\alpha}_{n'}, \quad (25b)$$

$$(\chi_{\mathrm{I,II}})_{m,n'} = \frac{-jk_m}{a^2}\left(\frac{1}{\beta_p^2} - \frac{1}{\beta_1^2}\right)\hat{\mathbf{u}}_m \cdot \boldsymbol{\alpha}_{n'}, \quad (25c)$$

and $\chi_{\mathrm{II,I}} = -\chi^T_{\mathrm{I,II}}$, where "$T$" denotes the transpose matrix. The formulas are exact within the approximation $\Phi_{p0}(\mathbf{r}|\mathbf{r}';\omega,\mathbf{k}) \approx \Phi_{p0}(\mathbf{r}|\mathbf{r}';\omega=0,\mathbf{k}=0)e^{-j\mathbf{k}\cdot(\mathbf{r}-\mathbf{r}')}$ [see formula (10)], which was used to evaluate the pertinent integrals. In the above, $f_V = \pi R^2/a^2$ is the volume fraction of the set of rods oriented along a fixed direction of space (e.g., the z direction), $k_m = \mathbf{k}\cdot\hat{\mathbf{u}}_m$ is the component of the wave vector along the $\hat{\mathbf{u}}_m$ direction, and β_1 and β_2 are constants (with unities of wave number) that only depend on the geometry of the structured material. The constant β_1 is such that[12]

$$\frac{1}{\beta_1^2} = 2\left(\frac{a}{2\pi}\right)^2 \sum_{l=1}^{\infty} \frac{\left[J_0\left(\frac{2\pi R}{a}l\right)\right]^2}{l^2}, \quad (26)$$

and the constant β_2 is

$$\frac{1}{\beta_2^2} = \frac{1}{\pi}\left(\frac{a}{2\pi}\right)^2 \sum_{m,n=-\infty}^{\infty} Q(\sqrt{m^2+n^2})\left[J_0\left(\frac{2\pi R}{a}\sqrt{m^2+n^2}\right)\right]^2, \quad (27a)$$

where the auxiliary function $Q(x)$ is defined by

$$Q(x) = \sum_{l=1}^{\infty}\frac{1}{l^2+x^2}\frac{1}{l^2} = \frac{3 + x^2\pi^2 - 3\pi x\coth(\pi x)}{6x^4}. \quad (27b)$$

The dielectric function of the wire medium can now be obtained by substituting Eq. (25) into Eq. (24). In order to be consistent with the approximation used in the evaluation of the submatrices [Eq. (10)], the matrix $\chi_{\mathrm{I,I}} - \chi_{\mathrm{I,II}} \cdot \chi^{-1}_{\mathrm{II,II}} \cdot \chi_{\mathrm{II,I}}$ should be calculated by retaining only the powers of ω or k_m $(m=1,2,3)$ of order up to two. Since $\chi_{\mathrm{I,II}}$ is $o(\mathbf{k})$, this implies that we can consider the following approximation in Eq. (25b):

$$(\chi_{\mathrm{II,II}})_{m',n'} \approx \left[\frac{1}{a}\frac{1}{\varepsilon_m - 1}\frac{1}{f_V}\frac{1}{12} + \frac{1}{a^3}\left(\frac{1}{\beta_p^2} - \frac{1}{\beta_1^2}\right)\right]\delta_{m',n'}, \quad (28)$$

so that the submatrix $\chi_{\mathrm{II,II}}$ becomes diagonal. It is now straightforward to find that the dielectric function verifies

$$\hat{\mathbf{u}}_m \cdot \left(\frac{\bar{\bar{\varepsilon}}}{\varepsilon_0} - \bar{\bar{\mathbf{I}}}\right)^{-1} \cdot \hat{\mathbf{u}}_n = \frac{1}{\beta_1^2}\left(k_m k_n - \frac{\omega^2}{c^2}\delta_{m,n}\right) + \left[\frac{1}{\varepsilon_m - 1}\frac{1}{f_V} + \left(\frac{1}{\beta_p^2} - \frac{1}{\beta_1^2}\right)\left(k_m^2 - \frac{\omega^2}{c^2}\right)\right]\delta_{m,n} - \frac{1}{A}\frac{1}{a^3}\left(\frac{1}{\beta_p^2} - \frac{1}{\beta_1^2}\right)^2\left(k_m^2\delta_{m,n} - \frac{1}{3}k_m k_n\right), \quad (29a)$$

$$A = \frac{1}{a}\frac{1}{\varepsilon_m - 1}\frac{1}{f_V}\frac{1}{12} + \frac{1}{a^3}\left(\frac{1}{\beta_p^2} - \frac{1}{\beta_1^2}\right), \quad (29b)$$

where $m,n=1,2,3$, and $\delta_{m,n}$ is the Kronecker's δ symbol. The permittivity dyadic $\bar{\bar{\varepsilon}}$ can now be obtained by calculating the inverse of the dyadic $(\bar{\bar{\varepsilon}}/\varepsilon_0 - \bar{\bar{\mathbf{I}}})^{-1}$, but the resulting expression is too cumbersome to show here. It is, however, possible to obtain an elegant solution for $\bar{\bar{\varepsilon}}$ when the term $1/[12a(\varepsilon_m - 1)f_V]$ in Eq. (29b) is negligible as compared to the second term. It is shown in Appendix A that this simplification is very accurate at least for frequencies below the effective plasma frequency $\omega_{p,\mathrm{eff}}$ (to be defined rigorously later) of the structured material. Under this approximation it is possible to rewrite Eq. (29a) as follows:

$$\left(\frac{\bar{\bar{\varepsilon}}}{\varepsilon_0}-\bar{\bar{\mathbf{I}}}\right)^{-1}=\bar{\bar{\mathbf{I}}}\left(\frac{1}{\varepsilon_m-1}\frac{1}{f_V}-\frac{\omega^2}{\beta_p^2c^2}\right)+\frac{\mathbf{kk}}{3}\left(\frac{1}{\beta_p^2}+\frac{2}{\beta_1^2}\right) \tag{30}$$

or equivalently, calculating the inverse of the dyadic, it is found that

$$\frac{\bar{\bar{\varepsilon}}}{\varepsilon_0}=\bar{\bar{\mathbf{I}}}+\frac{1}{\frac{1}{\varepsilon_m-1}\frac{1}{f_V}-\frac{\omega^2}{\beta_p^2c^2}}\left(\bar{\bar{\mathbf{I}}}-\frac{\mathbf{kk}}{k^2+l_0\left(\frac{\beta_p^2}{\varepsilon_m-1}\frac{1}{f_V}-\frac{\omega^2}{c^2}\right)}\right), \tag{31a}$$

$$l_0=\frac{3}{1+2\beta_p^2/\beta_1^2}, \tag{31b}$$

where $k^2=\mathbf{k}\cdot\mathbf{k}$ and $\mathbf{kk}\equiv\mathbf{k}\otimes\mathbf{k}$ represents the dyadic (tensor) product of the two vectors. The above result is the generalization to plasmonic rods of the dielectric function obtained in Ref. 12 for PEC rods using a less systematic approach. It may be readily verified that in case of PEC rods, i.e., when $\varepsilon_m=-\infty$, the dielectric function reduces to the one derived in our earlier paper.[12] In Sec. V, we will discuss in detail the physics predicted by the homogenization model. In Secs. VI and VII, the theoretical model will be validated with full wave numerical simulations.

V. PLANE-WAVE SOLUTIONS

In order to characterize the plane-wave solutions in the homogenized wire medium, it is convenient to rewrite Eq. (31) in terms of transverse and longitudinal components,

$$\frac{\bar{\bar{\varepsilon}}}{\varepsilon_0}=\varepsilon_t(\omega)\left(\bar{\bar{\mathbf{I}}}-\frac{\mathbf{kk}}{k^2}\right)+\varepsilon_l(\omega,k)\frac{\mathbf{kk}}{k^2}, \tag{32a}$$

where

$$\varepsilon_t(\omega)=1+\frac{1}{\frac{1}{\varepsilon_m-1}\frac{1}{f_V}-\frac{\omega^2}{\beta_p^2c^2}}, \tag{32b}$$

$$\varepsilon_l(\omega,k)=1+\frac{1}{\frac{k^2}{l_0\beta_p^2}+\left(\frac{1}{\varepsilon_m-1}\frac{1}{f_V}-\frac{\omega^2}{\beta_p^2c^2}\right)}. \tag{32c}$$

Decomposition (32a) is characteristic of isotropic spatially dispersive materials with a center of symmetry.[24] The property $\varepsilon_t\neq\varepsilon_l$ confirms the nonlocal response of the artificial plasma. It is straightforward to verify that Eq. (32a) implies that the plane-wave solutions supported by the material can be classified into transverse modes (with polarization perpendicular to the wave vector $\mathbf{k}$) and a longitudinal mode (with polarization parallel to the wave vector $\mathbf{k}$). The effective permittivity seen by the transverse modes is $\varepsilon_t(\omega)$, whereas the permittivity seen by the longitudinal mode is $\varepsilon_l(\omega,k)$. Notice that unlike ε_t, the longitudinal component ε_l depends on the wave vector. The dispersion characteristic of the transverse modes is given by

$$k^2=\varepsilon_t(\omega)\frac{\omega^2}{c^2}\quad\text{(transverse modes)}, \tag{33}$$

whereas the dispersion characteristic of the longitudinal mode is

$$\varepsilon_l(\omega,k)=0\quad\text{(longitudinal mode)}. \tag{34}$$

Solving the dispersion characteristic of the longitudinal mode with respect to k, it may also be written as

$$k^2=l_0\left(\frac{\omega^2}{c^2}-\beta_p^2-\frac{\beta_p^2}{\varepsilon_m-1}\frac{1}{f_V}\right)\quad\text{(longitudinal mode)}. \tag{35}$$

One should keep in mind that the parameters l_0 and β_p depend exclusively on the geometrical parameters of the lattice, whereas the permittivity of the plasmonic rods depends on frequency: $\varepsilon_m=\varepsilon_m(\omega)$. It is particularly interesting to analyze the case where the metal follows a Drude dispersion model with

$$\varepsilon_m=1-\frac{\omega_m^2}{\omega(\omega-j\Gamma)}, \tag{36}$$

where ω_m is the plasma frequency and Γ is the damping frequency. This dispersion model will be assumed in the rest of this work, and may describe accurately the properties of noble metals in the infrared domain.[25] Substituting Eq. (36) into Eq. (32b), it is readily found that the effective permittivity seen by the transverse modes also follows a Drude dispersion model,

$$\varepsilon_t(\omega)=1-\frac{\omega_{p,\text{eff}}^2}{\omega(\omega-j\Gamma_{\text{eff}})}, \tag{37a}$$

where the effective plasma frequency, $\omega_{p,\text{eff}}$, and the effective damping frequency, Γ_{eff}, are given by

$$\frac{1}{\omega_{p,\text{eff}}^2}=\frac{1}{\omega_m^2f_V}+\frac{1}{\beta_p^2c^2}, \tag{37b}$$

$$\frac{\Gamma_{\text{eff}}}{\omega_{p,\text{eff}}}=\frac{\Gamma}{\omega_m}\frac{1}{\sqrt{f_V}}\frac{1}{\sqrt{1+\frac{\omega_m^2f_V}{\beta_p^2c^2}}}. \tag{37c}$$

The effective plasma frequency $\omega_{p,\text{eff}}$ depends both on the plasma frequency of the bulk metal as well as on the geometrical parameters of the lattice. Typically, $\omega_{p,\text{eff}}$ is much lower than the plasma frequency of the bulk metal ω_m, which reflects the fact that nanostructuring may yield a more transparent material.[26] There are two interesting limit cases. The first case corresponds to $\frac{1}{\omega_m\sqrt{f_V}}\ll\frac{1}{\beta_pc}$, or equivalently to $\frac{c}{\omega_mR}\ll\frac{\sqrt{\pi}}{\beta_pa}$. Since at terahertz and infrared frequencies the skin depth of noble metals is such that $\delta_s\approx c/\omega_m$, the first case is equivalent to $\frac{\delta_s}{R}\ll\frac{\sqrt{\pi}}{\beta_pa}$, which implies that $\delta_s/R\ll1$, i.e., the skin depth of the metal is much less than the radius of the rods, because typical values of the parameter β_p are such that

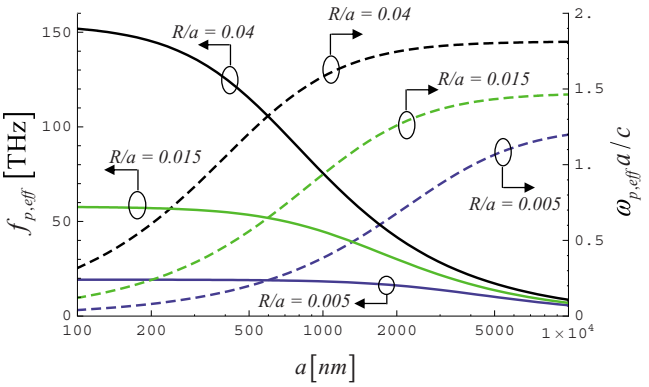

FIG. 2. (Color online) Plasma frequency of the artificial plasma, $f_{p,\mathrm{eff}}=\omega_{p,\mathrm{eff}}/2\pi$, as a function of the lattice constant a for silver wires and different values of R/a. The solid lines are associated with the left-hand side vertical scale, whereas the dashed lines are associated with the right-hand side scale. Notice that the horizontal scale has logarithmic unities.

$$1.0 < \beta_p a < 2.0 \quad (\text{for } 5\times 10^{-4} < R/a < 0.06). \quad (38)$$

In these circumstances the effective plasma frequency of the material is given by $\omega_{p,\mathrm{eff}} \approx \beta_p c$, where β_p is given by Eq. (9). In this regime, $\omega_{p,\mathrm{eff}}$ is roughly proportional to $1/a$ and is completely determined by the geometrical parameters of the structured material, R and a. From Eq. (38), it is clear that the electrical length of the unit cell at $\omega=\omega_{p,\mathrm{eff}}$ is relatively large. In fact, even though $\beta_p a$ decreases monotonically to zero with R/a, in practice, even for extremely thin wires, $\beta_p a$ remains fairly large because of the logarithmic dependence of Eq. (9) on R/a. This is a very important property since in order that the structured material can mimic the properties of a continuous material the electrical size of the unit cell should be a very small fraction of the operating wavelength. In Sec. VI, we will discuss with more detail how the failure to have $\omega_{p,\mathrm{eff}} a/c \ll 1$ may dramatically affect the electromagnetic response of the structured material. In the particular situation in which losses are small, $\Gamma_{\mathrm{eff}}/\omega_{p,\mathrm{eff}} \ll 1$, the metamaterial behaves basically in the same manner as the wire medium made of PEC rods studied in previous works.[12,13,15]

The second case of interest occurs when $\frac{1}{\omega_m\sqrt{f_V}} \gg \frac{1}{\beta_p c}$, or equivalently when the skin depth of the metal is much larger than the radius of the rods $\delta_s/R \gg 1$. In such scenario $\omega_{p,\mathrm{eff}} \approx \omega_m\sqrt{f_V}$, i.e., the effective plasma frequency is completely determined by the plasma frequency of the metal and by the volume fraction of the rods. Thus, in this regime it may possible to control the plasma frequency of the artificial material solely by adjusting the volume fraction of the metal. This property suggests very interesting possibilities: in fact, since f_V only depends on the ratio R/a, the electrical length of the unit cell $\omega_{p,\mathrm{eff}} a/c$ may be made arbitrarily small by making the lattice constant smaller and smaller, keeping the metal fill fraction invariant.

In order to illustrate these properties and the continuous transition between the two considered limit cases, in Fig. 2 we plot the plasma frequency as a function of the lattice constant a (solid lines), assuming that the ratio R/a is kept constant (the metal volume fraction is invariant). It is assumed that the metallic wires are made of silver, which following the experimental data tabulated in Ref. 25, may be characterized at terahertz and infrared frequencies by a Drude dispersion model with $\omega_m/2\pi=2175$ THz and $\Gamma_m/2\pi=4.35$ THz. It is seen in Fig. 2 that the effective plasma frequency increases monotonically as a is reduced from 10 μm down to 100 nm. However, consistent with the previous discussion, for some value of a the plasma frequency tends to saturate and does not vary appreciably as the lattice constant is further reduced. This corresponds to the regime where $\omega_{p,\mathrm{eff}} \approx \omega_m\sqrt{f_V}$. For convenience of the reader, we also plotted in Fig. 2 the electrical length of the unit cell, $\omega_{p,\mathrm{eff}} a/c$, as a function of the lattice constant (dashed lines associated with right-hand side vertical scale). It may be noticed that as soon as the effective plasma frequency starts to saturate, the electrical length of the unit cell may be dramatically reduced, and the lattice constant may become a very small fraction of the wavelength at $\omega=\omega_{p,\mathrm{eff}}$. Hence, the plasmonic properties of the metal may radically change the electromagnetic response of the material and may enable the realization of artificial plasmas at terahertz and infrared frequencies that imitate more closely the properties of metals near their plasma frequencies.

It is also important to discuss the effect of metallic loss in the structured material. Using the approximate identity for the skin depth, $\delta_s \approx c/\omega_m$, Eq. (37c) may be rewritten as

$$\frac{\Gamma_{\mathrm{eff}}}{\omega_{p,\mathrm{eff}}} \approx \frac{\Gamma}{\omega_m}\frac{1}{\sqrt{f_V}}\frac{1}{\sqrt{1+\dfrac{\pi}{(\beta_p a)^2}\left(\dfrac{R}{\delta_s}\right)^2}}. \quad (39)$$

Since the typical range of $\beta_p a$ is as in Eq. (38), the above formula shows that when $R/\delta_s \gg 10$ the ratio between the damping and plasma frequencies of the effective medium may be much smaller than the same ratio in the bulk metal even if f_V is very small. In such circumstances the loss in the effective medium may be negligible and the metallic rods may operate nearly as perfectly conducting wires, in the same manner as conventional wire media at microwaves.[12,13,15]

As mentioned before, the case $R/\delta_s \ll 1$ is especially interesting since it may enable the design of artificial plasmas with a lattice constant much smaller than the operating wavelength. In this regime it is clear that $\frac{\Gamma_{\mathrm{eff}}}{\omega_{p,\mathrm{eff}}} \approx \frac{\Gamma}{\omega_m}\frac{1}{\sqrt{f_V}}$, i.e., the ratio between the damping and plasma frequencies is enhanced in the artificial plasma by a factor of $1/\sqrt{f_V}$ as compared to the bulk metal. Since, in the regime $R/\delta_s \ll 1$ the effective plasma frequency is such that $\omega_{p,\mathrm{eff}} \approx \omega_m\sqrt{f_V}$, it follows that $\Gamma_{\mathrm{eff}} \approx \Gamma$, i.e., the absolute value of the damping frequency is nearly the same in the bulk metal and in the structured material. It is thus clear that the effect of loss will be increasingly important when the effective plasma frequency is made smaller. Nevertheless, since noble metals are characterized by $\Gamma/\omega_m \ll 1$ [e.g., for silver $\Gamma/\omega_m=0.002$ (Ref. 25)], the value of loss in the structured material may be fairly low even if $f_V \ll 1$. In Fig. 3 $\Gamma_{\mathrm{eff}}/\omega_{p,\mathrm{eff}}$ is plotted as a function of the lattice constant for the same parameters as in Fig. 2. It is seen that $\Gamma_{\mathrm{eff}}/\omega_{p,\mathrm{eff}}$ may increase significantly as

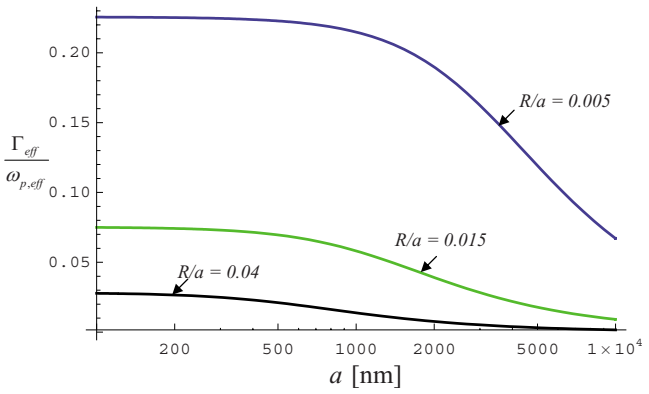

FIG. 3. (Color online) Normalized damping frequency of the artificial plasma, Γ_{eff}, as a function of the lattice constant a for silver wires and different values of R/a. Notice that the horizontal scale has logarithmic unities.

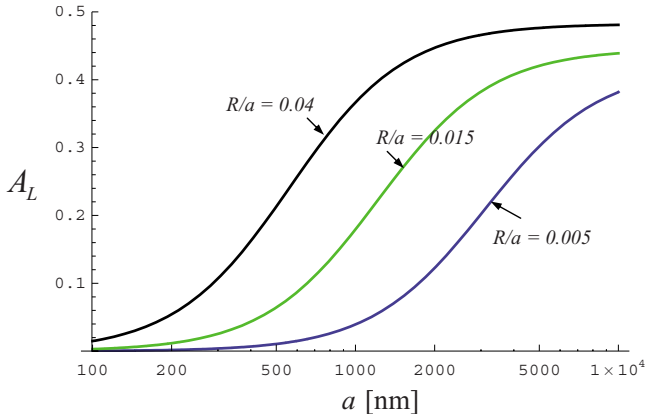

FIG. 4. (Color online) Slope of the longitudinal-mode dispersion, A_L, as a function of the lattice constant a for silver wires and different values of R/a. Notice that the horizontal scale has logarithmic unities.

the lattice constant is reduced, or equivalently (since for each curve the metal filling ratio is kept constant), as the radius of the rods is made smaller. Anyway, the value of $\Gamma_{\text{eff}}/\omega_{p,\text{eff}}$ remains fairly low even for values of R/a as small as $R/a=0.005$. Notice that at $\omega=\omega_{p,\text{eff}}$ the effective permittivity seen by the transverse modes is $\varepsilon_t \approx -j\Gamma_{\text{eff}}/\omega_{p,\text{eff}}$. Quite interestingly, even in the regime $R/\delta_s \ll 1$ for which $\Gamma_{\text{eff}}/\omega_{p,\text{eff}} \gg \Gamma/\omega_m$, the value of the imaginary part of the effective permittivity of the artificial material near $\omega_{p,\text{eff}}$ may be smaller than the value of the imaginary part of bulk silver near its plasma frequency. In fact, one should keep in mind that silver can be characterized using model (36) only at infrared and longer wavelengths, while at optical frequencies its characteristic loss may be significantly higher than that predicted by Eq. (36) due to interband absorptions.[27]

It is also relevant to study how the plasmonic effects affect the properties of the longitudinal mode. Assuming as before that the complex permittivity of the metal follows Drude characteristic (36), and neglecting for simplicity the effect of loss ($\Gamma \approx 0$) the dispersion characteristic of the longitudinal mode [Eq. (35)] can be rewritten as follows:

$$\omega^2 = \omega_{p,\text{eff}}^2 + A_L k^2 c^2, \quad A_L = \frac{\omega_{p,\text{eff}}^2}{\beta_p^2 c^2} \frac{1}{l_0}. \tag{40}$$

Ideally, for a local isotropic plasma the coefficient A_L should be such that $A_L \approx 0$ so that the dispersion characteristic of the longitudinal mode would be a flat line. As proven in Refs. 12 and 15 such an ideal situation is not verified for a wire medium formed by an array of PEC wires, and the dispersion characteristic of the longitudinal mode depends appreciably on k. As a consequence, both the transverse and the longitudinal modes may be excited at the interface of the artificial plasma. This is undesired because the longitudinal mode may significantly modify the response of the material. In order to understand how the plasmonic properties of the metal affect the response of the longitudinal mode, in Fig. 4 the coefficient A_L is plotted as a function of the lattice constant. As seen, when the lattice constant is fairly large so that $R/\delta_s \gg 1$ the slope of the longitudinal mode is relatively large, consistent with the results of Refs. 12 and 15. However, as the lattice constant and the radius of the rods are made smaller, the slope A_L may also become quite small. In particular, comparing with Fig. 2, it can be seen that for the range of parameters for which the electrical length of the unit cell $\omega_{p,\text{eff}} a/c$ verifies $\omega_{p,\text{eff}} a/c \ll 1$, the slope A_L may be negligible, and consequently it is expected that in this regime the effects of the longitudinal model become of less importance. This property further supports that the plasmonic properties of the bulk metal may enable the realization of structured materials with properties similar to those of metals near their plasma frequencies.

It is interesting to note that this conclusion is consistent with the results in Ref. 15, where it is suggested that the effects of spatial dispersion can be tamed by increasing the inductance of the metallic wires. In fact, it is known (see, for example, Ref. 28) that when the plasmonic properties of metal become relevant, the inductance becomes the sum of two components: the "geometrical" inductance and the "kinetic" inductance. The kinetic inductance is directly related to the plasmonic properties of the metal and contributes to increase the inductance of the system in the infrared domain, and in this way to reduce spatial dispersion effects.

VI. SUPERLENSING WITH AN ARTIFICIAL PLASMA SLAB

Perhaps the most distinguished application of metamaterials is superlensing.[1] The perfect lens requires a material slab with both permittivity and permeability simultaneously negative;[1] however it is well known that even a thin slab of a material with no magnetic properties and permittivity $\varepsilon \approx -1$ may enable a superlensing effect due to the resonant excitation of surface-plasmon polaritons (SPPs).[1,2,29] The objective of this section is to assess the possibility of achieving superlensing using an artificial plasma slab operated around the frequency for which $\text{Re}\{\varepsilon_t\}=-1$, and at the same time to validate the homogenization model introduced in Sec. IV. To this end, first we need to characterize the electromagnetic response of a planar slab with thickness L under plane-wave excitation. The geometry of the problem is depicted in the

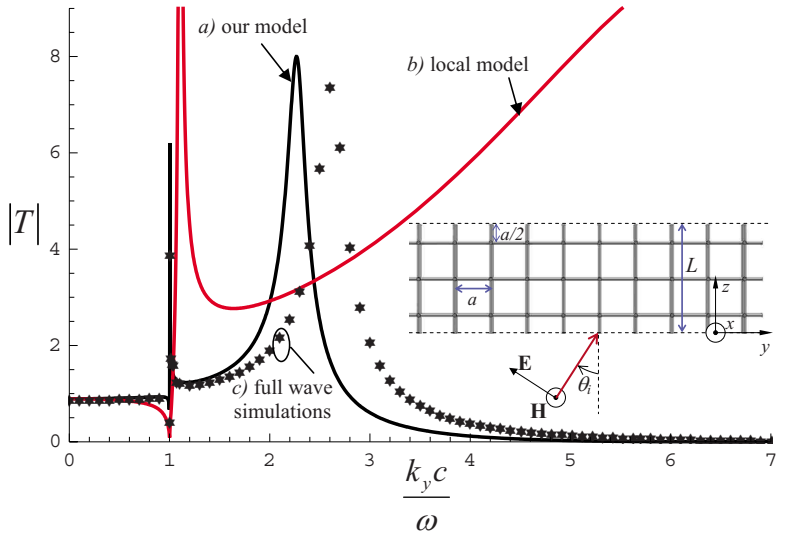

FIG. 5. (Color online) Amplitude of the transmission coefficient as a function of the (normalized) transverse wave vector, k_y, for $a=276$ nm and $R=0.03a$ at $f=76.1$ THz. The wire medium slab is formed by silver rods and has thickness $L=a=0.07\lambda_0$. (a) Nonlocal homogenization theory [Eq. (41)]. (b) Local model (effect of the longitudinal mode is neglected). (c) "Star"-shaped symbols: full wave simulations obtained with CST MICROWAVE STUDIO (Ref. 32). The inset represents the geometry of the problem in a hypothetical case where $L=3a$.

inset of Fig. 5. The metamaterial slab is periodic along the xoy plane and has a finite (integer) number of cells along the z direction. The interfaces are formed in such manner that the distance between the interfaces and the nearest wire plane (parallel to the xoy plane) is $a/2$. The geometry depicted in the inset of Fig. 5 corresponds to the case where the metamaterial slab is three cell thick. The incoming wave is transverse magnetic (TM) relatively to the interface, and the angle of incidence is θ_i. It is assumed that the incident magnetic field is along the x direction. The incoming wave can excite both the transverse and the longitudinal modes in the wire medium. Due to this reason, the solution of the scattering problem using homogenization theory is not straightforward and requires the use of an additional boundary condition.[30,31] These ideas are developed in Appendix B, where we demonstrate that the transmission coefficient $T=T(\omega,k_y)$ is given by

$$T=\frac{1}{1+\left(\frac{1}{\varepsilon_h}-\frac{1}{\varepsilon_t}\right)\frac{k_y^2}{k_z^{(L)}\gamma_0}\tan\left(\frac{k_z^{(L)}L}{2}\right)-\frac{k_z^{(T)}}{\varepsilon_t\gamma_0}\tan\left(\frac{k_z^{(T)}L}{2}\right)}-\frac{1}{1-\left(\frac{1}{\varepsilon_h}-\frac{1}{\varepsilon_t}\right)\frac{k_y^2}{k_z^{(L)}\gamma_0}\cot\left(\frac{k_z^{(L)}L}{2}\right)+\frac{k_z^{(T)}}{\varepsilon_t\gamma_0}\cot\left(\frac{k_z^{(T)}L}{2}\right)}. \tag{41}$$

In the above, k_y is the component of the incident wave vector parallel to the interface [$k_y=(\omega/c)\sin\theta_i$ for a propagating plane wave], $\gamma_0=\sqrt{k_y^2-(\omega/c)^2}$, ε_h is the relative permittivity of the host medium that supports the metallic wires, ε_t is the relative effective permittivity seen by the transverse modes in the artificial plasma, and $k_z^{(T)}$ and $k_z^{(L)}$ are the propagation constants along z associated with the transverse and longitudinal modes, respectively. If the wires are embedded in a host material with $\varepsilon_h=1$, the permittivity $\varepsilon_t(\omega)$ is given by Eq. (32b). In the general case where $\varepsilon_h\neq 1$, the transverse permittivity should be defined as

$$\varepsilon_t(\omega)=\varepsilon_h+\frac{1}{\frac{1}{\varepsilon_m-\varepsilon_h}\frac{1}{f_V}-\frac{\omega^2}{\beta_p^2c^2}}. \tag{42}$$

The propagation constants $k_z^{(T)}$ and $k_z^{(L)}$ are obtained by solving the plane-wave dispersion equation. It is found that [in the particular case $\varepsilon_h=1$, these formulas follow immediately from Eqs. (33) and (35)]

$$k_z^{(T)}=\sqrt{\varepsilon_t(\omega)\frac{\omega^2}{c^2}-k_y^2}, \tag{43a}$$

$$k_z^{(L)}=\sqrt{l_0\left(\frac{\omega^2}{c^2}\varepsilon_h-\beta_p^2-\frac{\beta_p^2}{\varepsilon_m/\varepsilon_h-1}\frac{1}{f_V}\right)-k_y^2}. \tag{43b}$$

From formula (41), it readily follows that the effects of the longitudinal mode are negligible if $k_z^{(L)}\to\infty$. In such limit case, Eq. (41) yields the transmission coefficient for a local material characterized by permittivity (42).

In the first example, we consider a material slab with thickness $L=a$, where $a=276$ nm is the lattice constant ($\omega_m a/c=2.0\times 2\pi$, where $\omega_m/2\pi=2175$ THz) and $R=0.03a$ is the radius of the rods. It is assumed that the metal wires are made of silver and that the host medium is air ($\varepsilon_h=1$). The condition $\mathrm{Re}\{\varepsilon_t\}=-1$ occurs at $f=76.1$ THz (the corresponding complex permittivity is $\varepsilon_t\approx -1-0.1j$; the

permittivity of silver is $\varepsilon_{Ag} \approx -810 - 50j$). Notice that the imaginary part of the transverse permittivity is relatively small at the design frequency, despite the radius being very small. The thickness of the slab is only $L=0.07\lambda_0$ at the frequency of interest. Since $L=a$, the lattice constant is also a very small fraction of the operating wavelength. As discussed in Sec. V, this is only possible because the radius of the rods is smaller than the skin depth of silver, and thus the plasmonic properties of metal play a major role.

In Fig. 5, the amplitude of the transmission characteristic $T=T(k_y)$ is shown. Notice that the transmission coefficient $T=T(k_y)$ may be regarded as the ("optical") transfer function of the structured material slab. For $|k_y c/\omega| < 1$ the incident wave is a propagating plane wave, whereas if $|k_y c/\omega| > 1$ the incident wave is an evanescent mode (component of the subwavelength spatial spectrum). The effect of metallic loss in silver is fully considered in the plots of Fig. 5.[25] The results obtained using the proposed homogenization theory [Eq. (41)] are represented in curve (a) (black solid line). It is seen that the transfer function has two sharp resonances around $k_y c/\omega \approx 1.0$ and $k_y c/\omega \approx 2.1$, which correspond to the resonant excitation of guided modes of the structured material. These guided modes closely mimic the role of surface plasmons in a thin silver film at optical frequencies. In particular, it may be seen that evanescent waves with transverse wave number such that $k_y c/\omega \approx 2.1$ are significantly enhanced by the metamaterial slab, possibly enabling a superlensing effect.[1,2,29] Despite, the effect of losses the amplitude of the transmission coefficient may be as large as $|T| \approx 8$ around $k_y c/\omega \approx 2.1$.

These results compare well with full wave simulations obtained with CST MICROWAVE STUDIO (Ref. 32) (discrete star-shaped symbols), which supports the validity of the homogenization results. CST MICROWAVE STUDIO models a single unit cell of the structure, and enforces periodic boundary conditions along the x direction and the Floquet-Bloch condition along the y direction (with phase shift determined by the angle of incidence). "Waveguide ports" are placed at $z=$const. planes located at a distance $1.5a$ from the two interfaces, and are used to excite the incoming plane wave and absorb the scattered fields. The transmission and reflection coefficients are computed using the frequency domain solver of CST MICROWAVE STUDIO.[32] These results can be regarded as the exact solution of the problem, apart from inevitable "numerical noise" intrinsic to all numerical methods.

We have also calculated the transfer function of a fictitious material slab described by a local permittivity model following Eq. (42) [curve (b) plotted with a red solid line]. As seen in Fig. 5, the local model predicts a much greater enhancement of evanescent modes as compared to the actual response of the structured material. This shows that despite the radius of rods being smaller than the skin depth of the metal, the effects of the longitudinal mode are still tangible. Notice that ideally the transfer function should be a growing exponential [consistent with curve (b)], $T \sim e^{k_y L}$,[1,2] in order that the attenuation in the free-space regions is compensated by the lens.

In order to investigate the possibility of reducing more significantly the nonlocal effects, we have studied an hypothetical geometry in which the lattice constant and the radius

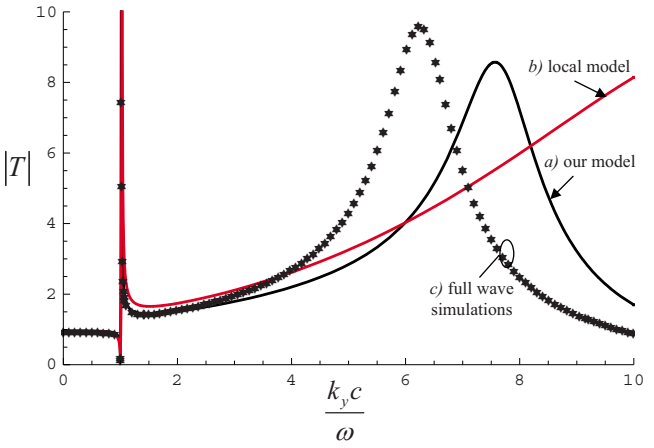

FIG. 6. (Color online) Transmission characteristic for $a=27.6$ nm ($\omega_m a/c = 0.2\times 2\pi$) and $R=0.03a$ at $f=81.7$ THz for a slab with $L=5a=0.038\lambda_0$. The legend is as in Fig. 5.

of the rods are reduced by a factor of ten so that $a=27.6$ nm ($\omega_m a/c = 0.2\times 2\pi$) and $R=0.03a$. The metal fill fraction is kept invariant as compared to the previous example. The actual fabrication of this structure would be quite challenging since the diameter of the wires is only 1.66 nm. Moreover, it is assumed here that such thin rods can be described by the same permittivity as bulk silver and that quantum-mechanical effects are negligible, but actually, as discussed ahead, such hypotheses may not be realistic (the possible effects of spatial dispersion in silver are studied in Appendix D). As proven in Sec. V, with very thin wires it may be possible to enhance the plasmonic properties of the metal and in this way minimize nonlocal effects. The frequency for which $\mathrm{Re}\{\varepsilon_t\}=-1$ is now $f=81.7$ THz. The permittivity of the wire medium is kept approximately the same as in the previous example, $\varepsilon_t \approx -1-0.1j$, because the volume fraction of the metal is invariant, and consequently the effective damping frequency normalized to the effective plasma frequency remains nearly unchanged (see Fig. 3). The permittivity of silver at $f=81.7$ THz is approximately $\varepsilon_{Ag} \approx -710-38j$. Notice that even though the lattice constant has decreased ten times, the frequency at which $\mathrm{Re}\{\varepsilon_t\}=-1$ has increased very modestly. As discussed in Sec. V, this happens because in the regime where the plasmonic properties dominate, the effective plasma frequency is nearly independent of a and only depends on the fill fraction of the metal: $\omega_{p,\mathrm{eff}} \approx \omega_m \sqrt{f_V}$. An important outcome of this property is that the electrical size of unit cell also decreases nearly by a factor of 10: $a=0.075\lambda_0$. We consider that the wire medium slab is formed by five unit cells so that the thickness is $L=5a=0.038\lambda_0$.

In Fig. 6, we represent the calculated transmission coefficient as a function of k_y. Now the theoretical model [curve (a)] predicts that the transmission characteristic has a sharp resonance around $k_y c/\omega \approx 7.5$ (besides the very narrow resonance close to $k_y c/\omega \approx 1.0$). The results obtained using CST MICROWAVE STUDIO (discrete star-shaped symbols) are relatively similar to those obtained with the theoretical model, apart from a slight shift of the resonance peak. It may also be seen that for a relatively large range of values of k_y (roughly

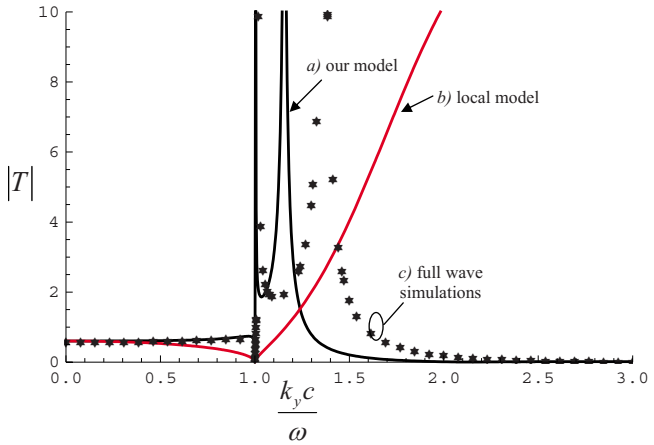

FIG. 7. (Color online) Transmission characteristic for $a=1.38$ μm ($\omega_m a/c=10.0\times 2\pi$) and $R=0.03a$ at $f=36.9$ THz for a slab with $L=a=1.17\lambda_0$. The legend is as in Fig. 5.

for $k_y c/\omega<6.0$), the response of the structured material is very similar to that of local material with permittivity given by Eq. (42). This demonstrates that by using thin rods with radius much smaller than the skin depth of the metal, it could be possible to nearly eliminate the spatial dispersion effects, and in this way design a structured subwavelength film that might enable a superlensing effect at infrared frequencies. However, it is also quite evident from our analysis that to obtain such good performance using silver rods is most likely impossible since the required radius of the rods is extremely small. Indeed, since the skin depth of silver is only a few tenths of nanometers at infrared frequencies, the required rods radius is only a few nanometers. Such ultrathin metallic objects most likely cannot be described using the same permittivity model as bulk silver and may behave as objects with positive permittivity. This may be an insurmountable fundamental obstacle to achieve superlensing with this structured material. Using a metal or a semiconductor with a smaller plasma frequency (and thus larger skin depth) may however allow using rods with larger radii, but a definite conclusion about this possibility requires further studies.

The described regime is radically different from the one in which the plasmonic properties of the metal are negligible. To illustrate this we consider a design example in which $a=1.38$ μm ($\omega_m a/c=10.0\times 2\pi$) and $R=0.03a$, i.e., the lattice constant is increased five times as compared to the first example, while the metal fill fraction is maintained. For these parameters it may be easily verified that the skin depth of the metal becomes smaller than the radius of the wires. The frequency for which $\mathrm{Re}\{\varepsilon_t\}=-1$ is now $f=36.9$ THz ($\varepsilon_t\approx -1-0.05j$; $\varepsilon_{\mathrm{Ag}}\approx -3400-400j$). As expected, when the conducting properties of the metallic wires are improved the effect of metallic loss becomes less significant. Notice that very differently from the second example, the frequency of operation suffers a significant variation in the present example. This effect was discussed in Sec. V, and is consistent with the results of Fig. 2. The electric size of the unit cell is now as large as $a=0.17\lambda_0$. The wire medium slab is assumed to be one cell thick: $L=a=0.17\lambda_0$.

The transmission characteristic of the considered structure is shown in Fig. 7. It can be seen that the results are dramatically different from those of the previous example (notice the different span of the horizontal scales). Indeed, as soon as conductive properties of the metal improve and the skin depth becomes smaller than the radius of the wires, both resonance peaks occur relatively close to $k_y c/\omega\approx 1.0$ and are extremely narrow. Hence, only evanescent modes with relatively small values of k_y can be enhanced by the wire medium slab. It is clear that this property precludes any significant superlensing effect, and shows how different is the performance of the metamaterial in the regime where the metal behaves as a good conductor. To conclude this section, we note that the results obtained at microwaves using typical wire media designs are relatively similar to those of the last example, being the resonant peaks even closer to the point $k_y c/\omega\approx 1.0$.

VII. RESONANCES ABOVE THE PLASMA FREQUENCY

While in Sec. VI we were mostly interested in the regime where the wire medium may be used as a near-field lens and is characterized by $\varepsilon_t\approx -1$, here we will investigate its frequency response, primarily in the range where $\mathrm{Re}\{\varepsilon_t\}>0$. The main motivations for this study are the findings in Refs. 33 and 34, which demonstrated that thin films of alkali metals (e.g., sodium and potassium) may have a nonlocal electromagnetic response in many ways analogous to that of the wire medium considered here, and behave as nonlocal plasmas near their UV plasma frequencies. It was shown in Refs. 33 and 34 that the resonant excitation of longitudinal plasmons in thin alkali-metal films may result in observable oscillatory variations in the absorption, transmission, and reflection spectrum above the plasma frequency. It is thus natural to ask if due to spatial dispersion effects the wire medium considered here may be characterized by similar features.

The phenomenon identified in Ref. 33 can be easily understood by analyzing the formula of the transmission coefficient, given by Eq. (41). To begin with, let us temporarily neglect the effect of metallic loss so that above the effective plasma frequency, $\omega_{p,\mathrm{eff}}$, both $k_z^{(T)}$ and $k_z^{(L)}$ are real valued. For simplicity, we assume in this section that $\varepsilon_h=1$. It is simple to verify that in these conditions Eq. (43) yields $k_z^{(T)}=\sqrt{(\omega^2-\omega_{p,\mathrm{eff}}^2)/c^2-k_y^2}$ and $k_z^{(L)}=\sqrt{(\omega^2-\omega_{p,\mathrm{eff}}^2)/A_L c^2-k_y^2}$. As discussed in Sec. V, the parameter A_L is typically much less than unity, especially when the plasmonic effects in metal play a dominant role. Hence, it is clear that above the plasma frequency $k_z^{(L)}\gg k_z^{(T)}$. But this implies that in the first parcel in Eq. (41) the term associated with $\tan(k_z^{(L)}L/2)$ will vary much faster than the remaining terms in the same denominator, particularly at the frequency values such that $k_z^{(L)}L/2=(m+1/2)\pi$, $m=0,1,2,\ldots$ for which the first parcel of Eq. (41) must vanish. Similarly, in the second parcel of Eq. (41) the term associated with $\cot(k_z^{(L)}L/2)$ varies much faster than the remaining terms when $k_z^{(L)}L/2=m\pi$, $m=1,2,\ldots$, and the second parcel of Eq. (41) vanishes at these frequencies. Thus, Eq. (41) predicts that the transmission characteristic may have significant oscillations when $k_z^{(L)}L=n\pi$,

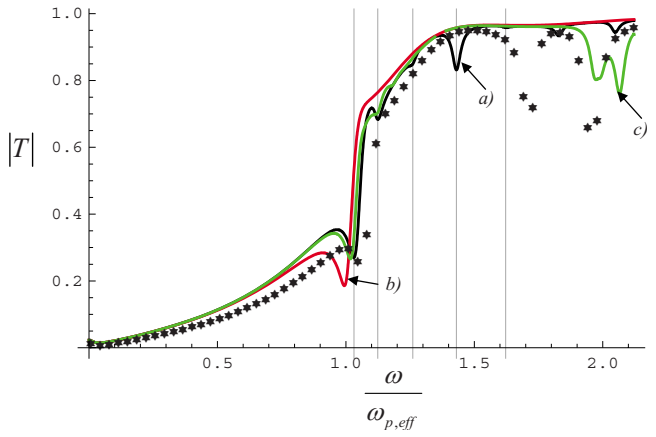

FIG. 8. (Color online) Transmission characteristic for $a=276$ nm ($\omega_m a/c=2.0\times 2\pi$) and $R=0.03a$ for a slab with $L=5a$. The angle of incidence is $\theta_i=15°$. The plasma frequency is $\omega_{p,\mathrm{eff}}/2\pi=107.6$ THz. (a) Nonlocal homogenization theory [Eq. (41)]. (b) Local model (effect of the longitudinal mode is neglected). (c) Nonlocal homogenization theory using the dielectric function defined by Eq. (29). The discrete star-shaped symbols correspond to full wave simulations obtained with CST MICROWAVE STUDIO (Ref. 32). The vertical gridlines mark the resonances predicted by Eq. (41) for $n=1$, 2, 3, 4, and 5.

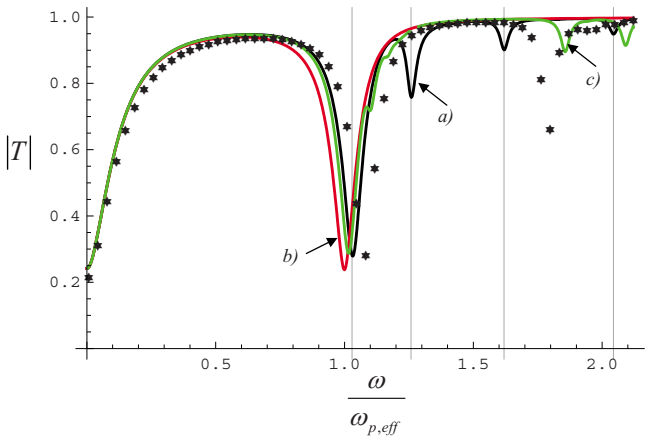

FIG. 9. (Color online) Transmission characteristic for $a=27.6$ nm ($\omega_m a/c=0.2\times 2\pi$) and $R=0.03a$ for a slab with $L=5a$. The angle of incidence is $\theta_i=45°$. The plasma frequency is $\omega_{p,\mathrm{eff}}/2\pi=115.6$ THz. The legend is as in Fig. 8. The vertical gridlines mark the resonances predicted by Eq. (41) for $n=1$, 3, 5, and 7.

$n=1,2,\ldots$, i.e., when the longitudinal mode verifies the Fabry-Pérot condition. Using $k_z^{(L)}=\sqrt{(\omega^2-\omega_{p,\mathrm{eff}}^2)/A_L c^2-k_y^2}$ and putting $k_y=(\omega/c)\sin\theta_i$ it is readily found that the resonance frequencies are

$$\omega_n=\sqrt{\frac{\omega_{p,\mathrm{eff}}^2+A_L\left(\frac{\pi}{L}n\right)^2c^2}{1-A_L\sin^2\theta_i}},\quad n=1,2,\ldots. \tag{44}$$

The above formula is only valid for small losses and when $\varepsilon_h=1$, and assumes that the metal follows Drude model (36). It is clear that in case of significant losses the oscillations in the transmission coefficient may become much weaker because the imaginary part of $k_z^{(L)}$ may severely damp the longitudinal mode.

In Fig. 8 we plot the calculated transmission coefficient as a function of frequency for a metamaterial slab with $a=276$ nm, $R=0.03a$, and $L=5a$. As in Sec. VI, it is assumed that the wires are made of silver. The angle of incidence is $\theta_i=15°$. Curve (a) (black solid line) corresponds to the transmission coefficient obtained using the nonlocal homogenization model [Eq. (41)], whereas curve (b) (red solid line) was calculated using a local homogenization model (the effect of the longitudinal mode is neglected). Consistent with the previous discussion, it is seen that above the effective plasma frequency the transmission characteristic predicted by the nonlocal model [curve (a)] has several oscillations. The first five resonant frequencies ($n=1$, 2, 3, 4, and 5) are marked in Fig. 8 with vertical gridlines. The local model [curve (b)] does not predict these multiple resonances. Using CST MICROWAVE STUDIO,[32] we have calculated the actual response of the metamaterial slab. Very disappointingly, it can be seen in Fig. 8 (star-shaped discrete symbols) that the full wave results only predicts the resonance associated with $n=1$, and that it does not predict any other resonances in the range $\omega/\omega_{p,\mathrm{eff}}<1.5$.

We obtained similar results for wire media with other geometrical parameters and for different angles of incidence. For instance, in Fig. 9 we show the transmission coefficient as a function of frequency for a wire medium slab with $a=27.6$ nm, $R=0.03a$, and $L=5a$. The angle of incidence is $\theta_i=45°$. The vertical gridlines mark the resonances corresponding to $n=1$, 3, 5, and 7. We do not show the resonances corresponding to n even since they are not perceptible. In fact, for n even the oscillations are associated with the second term in Eq. (41), which may be little sensitive to the variations in the term $\cot(k_z^{(L)}L/2)$ if the thickness of the slab is a very small fraction of the wavelength of operation λ_0, as in this example.

Despite the extremely small electrical length of the unit cell in the considered frequency range, it is seen in Fig. 9 that only the $n=1$ resonance of the transmission characteristic is confirmed by the full wave simulations. This seems to indicate that the homogenization model may not be so accurate above the effective plasma frequency. A possible justification is that the oscillations of the transmission coefficient correspond to values of $k_z^{(L)}$ relatively large. More specifically, for nth resonance we have that $k_z^{(L)}L=n\pi$ and thus $k_z^{(L)}a=n\pi a/L$ (in the considered examples $a/L=1/5$). Hence, for large n it is not true that $|k_z^{(L)}a|\ll\pi$, as assumed in the derivation of Sec. IV. Another possible justification is related to interface effects and to the granularity of the material, even though in principle these effects are very small for materials where the unit cell is a very small fraction of the operating wavelength, as in the examples considered here.

However, the lack of oscillations above the plasma frequency may be due to a different reason. As mentioned in Sec. IV, dielectric function (31) is only valid under the hypothesis that the term $1/[12a(\varepsilon_m-1)f_V]$ can be neglected in Eq. (29b). As shown in Appendix A, this is a quite accurate

approximation *below* the effective plasma frequency of the wire medium. However, from the results of Appendix A, it is clear that this approximation is not really justifiable above the plasma frequency, particularly when the plasmonic properties of the metallic wires play a dominant role. Due to this reason, we have studied if by taking into account the term $1/[12a(\varepsilon_m-1)f_V]$ in Eq. (29b) the electromagnetic response of the wire medium slab could be better predicted. The homogenization methods are quite similar to those used in the derivation of Eq. (41), and the main ideas are sketched in Appendix C. We only mention here that when $\bar{\bar{\varepsilon}}$ is defined consistently with Eq. (29), in general the electromagnetic modes cannot be classified as transverse and longitudinal waves, but instead are hybrid modes. The transmission characteristic obtained using the described formulation is plotted in Figs. 8 and 9 as curve (c) (solid green line). It is seen that curve (c) is practically coincident with curve (a) below the effective plasma frequency. However, above the plasma frequency curve (c) tends to follow more closely the full wave simulations obtained with CST MICROWAVE STUDIO, and does not predict significant oscillations of the transmission characteristic for $\omega<1.5\omega_{p,\mathrm{eff}}$, apart from the $n=1$ resonance close to the plasma frequency of the wire medium. We have verified that this property also holds for other examples not reported here. This suggests that above the plasma frequency it may be more accurate to describe the metamaterial using the dielectric function defined implicitly by Eq. (29) instead of using the simpler model (31).

VIII. CONCLUSION

In this paper, we derived the dielectric function of a connected wire medium, taking into account both the plasmonic properties and the loss in the metal. It was shown that the plasmonic properties of the metal may modify in a drastic manner the propagation properties of the structured material. It was proven that when the radius of the wires is made smaller than the skin depth of the metal, the electrical size of the unit cell may be a very small fraction of the wavelength at the effective plasma frequency, and the spatial dispersion effects may be relatively weak. This scenario is dramatically different from what happens in the microwave regime, where to a good approximation the metal can be described as a perfect conductor. It was shown that the effect of loss may be tolerable even for thin rods. We have characterized the transfer function of a wire medium slab when $\mathrm{Re}\{\varepsilon_t\}=-1$. It was demonstrated that unlike in the microwave regime, at infrared frequencies the subwavelength spectrum (i.e., evanescent waves) may be significantly enhanced by a thin slab. However, it looks quite difficult to obtain a significant superlensing effect using silver rods since it would require rods with very small radii (a few nanometers). Finally, motivated by the results reported in Refs. 33 and 34, we studied the frequency response of a wire medium slab and investigated the possible existence of oscillations in the transmission characteristic. To conclude we mention that the analysis of this work can be easily generalized to other configurations of wire media, like arrays of nonconnected wires.[35] In general, the ohmic connection between the wires is essential to avoid strong spatial dispersion effects characteristic of nonconnected wires.[12,35]

ACKNOWLEDGMENTS

This work was partially funded by Fundação para Ciência e a Tecnologia under Project No. PDTC/EEA-TEL/71819/2006.

APPENDIX A

In this appendix we show that for frequencies below the effective plasma frequency of the structured material, $\omega_{p,\mathrm{eff}}$, it is indeed possible to neglect the term $1/[12a(\varepsilon_m-1)f_V]$ in Eq. (29b). In fact, using Eq. (37b) and assuming small metallic losses ($\Gamma\approx 0$), it can be readily shown that

$$\frac{1}{|\varepsilon_m-1|}\frac{(\beta_p a)^2}{f_V}\frac{1}{12}=\frac{(\beta_p a)^2}{12}\frac{\omega^2}{\omega_{p,\mathrm{eff}}^2}\frac{1}{1+\dfrac{\omega_m^2 f_V}{\beta_p^2 c^2}} \leq \frac{(\beta_p a)^2}{12}\left(\frac{\omega}{\omega_{p,\mathrm{eff}}}\right)^2. \tag{A1}$$

But since the typical range of $\beta_p a$ is as in Eq. (38), the above equation shows that the leftmost expression is much smaller than unity when ω is below $\omega_{p,\mathrm{eff}}$ (this property is even better verified in case of metallic losses or when the radius of the rods is much larger than the skin depth of the metal). This result together with the fact that $\beta_1^2 \gg \beta_p^2$ proves that in these circumstances the term $1/[12a(\varepsilon_m-1)f_V]$ may be neglected in Eq. (29b).

APPENDIX B

Here, we describe the analytical model that enables the calculation of the transmission and reflection coefficients in the scattering problem formulated in Sec. VI. The geometry of the problem is shown in the inset of Fig. 5. Since the incident magnetic field is directed along the x direction, the magnetic field in all space is also along the x direction. The electromagnetic fields in the metamaterial slab can be written as a superposition of transverse and longitudinal modes. It is simple to verify that the magnetic field associated with the longitudinal mode vanishes. Therefore, assuming that the amplitude of the incoming magnetic field is normalized to unity, the magnetic field in all space is of the form (the y variation in the field is suppressed)

$$H_x = e^{-\gamma_0 z}+\mathrm{Re}^{\gamma_0 z}, \quad z<0, \tag{B1a}$$

$$H_x = A_1 e^{-jk_z^{(T)}z}+A_2 e^{jk_z^{(T)}z}, \quad 0<z<L, \tag{B1b}$$

$$H_x = Te^{-\gamma_0(z-L)}, \quad z>L, \tag{B1c}$$

where R and T are the reflection and transmission coefficients, $\gamma_0=\sqrt{k_y^2-(\omega/c)^2}$ [$k_y=(\omega/c)\sin\theta_i$ for a propagating incoming plane wave], $k_z^{(T)}$ is the propagation constant along z of the transverse mode in the wire medium, and A_1 and A_2 are unknown constants.

The electric field associated with a plane wave with magnetic field along the x direction and wave vector $\mathbf{k}=(0,k_y,k_z)$ is such that

$$\mathbf{E}=\frac{1}{\omega\varepsilon_0}\bar{\bar{\varepsilon}}_r^{-1}\cdot(\hat{\mathbf{u}}_x\times\mathbf{k})H_x, \tag{B2}$$

where $\bar{\bar{\varepsilon}}_r$ is the relative permittivity dyadic. Therefore, it is clear that the electric field associated with Eq. (B1) is such that

$$\mathbf{E}=\frac{1}{\omega\varepsilon_0}(\hat{\mathbf{u}}_x\times\mathbf{k}_0^+e^{-\gamma_0 z}+\hat{\mathbf{u}}_x\times\mathbf{k}_0^-\,\mathrm{Re}^{\gamma_0 z}),\quad z<0, \tag{B3a}$$

$$\mathbf{E}=\frac{1}{\omega\varepsilon_0\varepsilon_t(\omega)}(\hat{\mathbf{u}}_x\times\mathbf{k}_T^+A_1e^{-jk_z^{(T)}z}+\hat{\mathbf{u}}_x\times\mathbf{k}_T^-A_2e^{jk_z^{(T)}z})+\frac{1}{\omega\varepsilon_0}(B_1\mathbf{k}_L^+e^{-jk_z^{(L)}z}+B_2\mathbf{k}_L^-e^{jk_z^{(L)}z}),\quad 0<z<L, \tag{B3b}$$

$$\mathbf{E}=\frac{1}{\omega\varepsilon_0}T\hat{\mathbf{u}}_x\times\mathbf{k}_0^+e^{-\gamma_0(z-L)},\quad z>L. \tag{B3c}$$

In the above, $\mathbf{k}_0^{\pm}=(0,k_y,-(\pm j\gamma_0))$ is the wave vector in free-space, and $\mathbf{k}_T^{\pm}=(0,k_y,\pm k_z^{(T)})$ and $\mathbf{k}_L^{\pm}=(0,k_y,\pm k_z^{(L)})$ are the wave vectors associated with the transverse and longitudinal modes in the artificial plasma, respectively. Notice that inside the artificial plasma the electric field is the superposition of transverse and longitudinal waves. The unknown constants B_1 and B_2 are the amplitudes of the longitudinal waves. The permittivity seen by the transverse modes, $\varepsilon_t(\omega)$, is normalized to the permittivity of vacuum, and in the general case is given by Eq. (42). The propagation constants $k_z^{(T)}$ and $k_z^{(L)}$ are given by Eq. (43).

By matching the tangential components of the electromagnetic fields at the interfaces $z=0$ and $z=L$, the following equations are derived:

$$1+R=A_1+A_2, \tag{B4a}$$

$$T=A_1e^{-jk_z^{(T)}L}+A_2e^{jk_z^{(T)}L}, \tag{B4b}$$

$$(-\gamma_0)(1-R)=\frac{1}{\varepsilon_t}(-jk_z^{(T)})(A_1-A_2)+jk_y(B_1+B_2), \tag{B4c}$$

$$(-\gamma_0)T=\frac{1}{\varepsilon_t}(-jk_z^{(T)})(A_1e^{-jk_z^{(T)}L}-A_2e^{jk_z^{(T)}L})+jk_y(B_1e^{-jk_z^{(L)}L}+B_2e^{jk_z^{(L)}L}). \tag{B4d}$$

These four equations are clearly insufficient to determine the six unknowns (R, T, A_1, A_2, B_1, and B_2). It is know that this property is a consequence of spatial dispersion effects, and that to obtain a well-formed system we need to consider an additional boundary condition (ABC).[30,31] Quite interestingly, this property is not specific of the structured materials under study here, and thin films of alkali metals such as sodium and potassium may also require the use of an auxiliary boundary condition.[33] In Ref. 33, it was shown that in materials where a longitudinal bulk plasma wave can propagate, the classical boundary conditions are insufficient to solve a scattering problem, and the microscopic currents should vanish at the interface. Similar ideas were recently used in Ref. 15 to characterize a wire medium with the same topology as the one considered here. These ideas are consistent with the results of our earlier works,[30,31] where we have proven that for an array of parallel metallic wires the annulment of the microscopic electric current along the wires implies the continuity of $\varepsilon_h(z)E_z$, where ε_h is the permittivity of the host material (which may differ at both sides of the interface) and E_z is the component of the macroscopic electric field normal to the interface. We will use the same boundary condition to characterize the material under study. The equations corresponding to the continuity of $\varepsilon_h(z)E_z$ at the interfaces are

$$k_y(1+R)=\frac{\varepsilon_h}{\varepsilon_t}k_y(A_1+A_2)+\varepsilon_h k_z^{(L)}(B_1-B_2), \tag{B4e}$$

$$k_yT=\frac{\varepsilon_h}{\varepsilon_t}k_y(A_1e^{-jk_z^{(T)}L}+A_2e^{jk_z^{(T)}L})+\varepsilon_h k_z^{(L)}(B_1e^{-jk_z^{(L)}L}-B_2e^{jk_z^{(L)}L}). \tag{B4f}$$

Solving the linear system Eq. (B4) with respect to the unknowns, we may easily determine the transmission and reflection coefficients. It can be proven that the transmission coefficient T may be written in close analytical form as in Eq. (41). A similar formula may also be written for R, but it is not shown here for conciseness. It may be verified that in the lossless case [$\bar{\bar{\varepsilon}}(\omega,\mathbf{k})$ is real for $\mathbf{k}$ real] the proposed ABC ensures the conservation of energy, more specifically that $|T|^2=1-|R|^2$ for a propagating incident wave.

APPENDIX C

Here, we briefly explain how the reflection and transmission coefficients are calculated in the general case where the wire medium is characterized using a dielectric function defined consistently with Eq. (29), i.e., without neglecting the term $1/[12a(\varepsilon_m-1)f_V]$ in Eq. (29b). In this general case, the plane-wave solutions supported by the structured material cannot be decomposed into transverse and longitudinal waves as in Sec. V. It may be verified that for propagation in the yoz plane (with $k_x=0$) the artificial plasma supports two electromagnetic modes with propagation constants along z, given by $k_z^{(1)}=k_z^{(1)}(\omega,k_y)$ and $k_z^{(2)}=k_z^{(2)}(\omega,k_y)$. These two modes may be regarded as quasitransverse and quasilongitudinal modes, respectively. The propagation constants may be calculated by solving the standard dispersion characteristic for plane waves with $\bar{\bar{\varepsilon}}$ defined as in Eq. (29),[24] but the formulas are omitted here for brevity. The magnetic field inside the structured material is now written as [compare with Eq. (B1)]

$$H_x = A_1 e^{-jk_z^{(1)}z} + A_2 e^{jk_z^{(1)}z} + B_1 e^{-jk_z^{(2)}z} + B_2 e^{jk_z^{(2)}z}, \quad 0 < z < L \tag{C1}$$

for some constants A_1, A_2, B_1, and B_2. The magnetic field in the air regions is defined as in Eq. (B1). Notice that in the scenario considered here the magnetic field has a contribution from both the quasitransverse and the quasilongitudinal modes. The electric field associated with Eq. (C1) can be easily obtained by applying formula (B2) to each of the terms (i.e., plane waves) associated with the magnetic field. The reflection and transmission coefficients are computed by matching the fields H_x and E_y at the interfaces, and by enforcing the additional boundary condition, i.e., by ensuring the continuity of $\varepsilon_h(z)E_z$.

APPENDIX D

Here, we estimate the spatial dispersion in the permittivity of bulk silver, and discuss its possible effect on the properties of the structured material under study. It is well known that real metals are spatially dispersive, and thus may support a longitudinal mode as well as transverse modes. The dispersion of the longitudinal mode in a metal may be estimated using the "hydrodynamic model" [compare with Eq. (40)],

$$\omega^2 = \omega_m^2 + \tilde{A}_L k^2 c^2, \tag{D1}$$

where ω_m is the plasma frequency of the metal, and $\tilde{A}_L = \frac{3}{5}(\frac{v_F}{c})^2$, where v_F is the Fermi velocity.[17,33] For silver the parameter $\tilde{A}_L$ may be estimated to be $\tilde{A}_L \approx 1.5 \times 10^{-5}$.[17] Thus, the attenuation of the longitudinal mode below the plasma frequency ω_m is $\gamma_L = \sqrt{(\omega_m^2 - \omega^2)/(c^2 \tilde{A}_L)}$. Notice that γ_L is much larger than the attenuation constant of transverse modes, γ_T (by a factor of $1/\sqrt{\tilde{A}_L}$). Thus, it is reasonable to assume that spatial dispersion may be neglected provided $\gamma_L d \gg 1$, where d is some characteristic dimension of the material. This condition ensures that the longitudinal mode is strongly attenuated and that there is no resonant coupling between two interfaces of the material. In case of metallic rods, one can choose d equal to the diameter of the rods, i.e., $d=2R$. But it is simple to verify that even for the most critical geometry considered in this work (silver rods with $d=1.66$ nm operated at 81.7 THz), we have $\gamma_L d = 19.5$, which is large enough to conclude that as long as the permittivity of bulk silver describes adequately the properties of the thin rods, the effects of spatial dispersion of bulk silver are expected to be negligible. The main reason for this property is that silver is operated well below its plasma frequency. It is important to emphasize that such conclusion is only valid as long as the permittivity of bulk silver can be used to characterize such ultrathin metallic obstacles.

*mario.silveirinha@co.it.pt

[1] J. B. Pendry, Phys. Rev. Lett. **85**, 3966 (2000).
[2] N. Fang, H. Lee, C. Sun, and X. Zhang, Science **308**, 534 (2005).
[3] T. Taubner, D. Korobkin, Y. Urzhumov, G. Shvets, and R. Hillenbrand, Science **313**, 1595 (2006).
[4] D. R. Smith, Willie J. Padilla, D. C. Vier, S. C. Nemat-Nasser, and S. Schultz, Phys. Rev. Lett. **84**, 4184 (2000).
[5] M. Silveirinha and N. Engheta, Phys. Rev. Lett. **97**, 157403 (2006).
[6] N. Engheta, Science **317**, 1698 (2007).
[7] J. Brown, Proc. IEE, pt. 4 **100**, 51 (1953).
[8] W. Rotman, IRE Trans. Antennas Propag. **10**, 82 (1962).
[9] J. B. Pendry, A. J. Holden, W. J. Stewart, and I. Youngs, Phys. Rev. Lett. **76**, 4773 (1996).
[10] D. F. Sievenpiper, M. E. Sickmiller, and E. Yablonovitch, Phys. Rev. Lett. **76**, 2480 (1996).
[11] P. A. Belov, R. Marques, S. I. Maslovski, I. S. Nefedov, M. Silveirinha, C. R. Simovski, and S. A. Tretyakov, Phys. Rev. B **67**, 113103 (2003).
[12] M. G. Silveirinha and C. A. Fernandes, IEEE Trans. Microwave Theory Tech. **53**, 1418 (2005).
[13] M. A. Shapiro, G. Shvets, J. R. Sirigiri, and R. J. Temkin, Opt. Lett. **31**, 2051 (2006).
[14] M. Hudlicka, J. Machác, and I. S. Nefedov, PIER **65**, 233 (2006).
[15] A. Demetriadou and J. B. Pendry, J. Phys.: Condens. Matter **20**, 295222 (2008).
[16] A. Alù, A. Salandrino, and N. Engheta, Opt. Express **14**, 1557 (2006).
[17] R. Ruppin, J. Phys.: Condens. Matter **17**, 1803 (2005).
[18] M. G. Silveirinha, Phys. Rev. E **73**, 046612 (2006).
[19] A. L. Pokrovsky and A. L. Efros, Phys. Rev. B **65**, 045110 (2002).
[20] M. G. Silveirinha, Phys. Rev. B **75**, 115104 (2007).
[21] M. G. Silveirinha, Phys. Rev. B **76**, 245117 (2007).
[22] M. G. Silveirinha, IEEE Trans. Antennas Propag. **56**, 390 (2008).
[23] V. Agranovich and V. Ginzburg, *Spatial Dispersion in Crystal Optics and the Theory of Excitons* (Wiley, New York, 1966).
[24] L. D. Landau and E. M. Lifshitz, *Electrodynamics of Continuous Media, Course of Theoretical Physics* (Elsevier, New York, 2004), Vol. 8, p. 360.
[25] M. A. Ordal, Robert J. Bell, R. W. Alexander, Jr., L. L. Long, and M. R. Querry, Appl. Opt. **24**, 4493 (1985).
[26] R. S. Bennink, Y.-K. Yoon, and R. W. Boyd, Opt. Lett. **24**, 1416 (1999).
[27] P. B. Johnson and R. W. Christy, Phys. Rev. B **6**, 4370 (1972).
[28] S. Tretyakov, Metamaterials **1**, 40 (2007).
[29] J. T. Shen and P. M. Platzman, Appl. Phys. Lett. **80**, 3286 (2002).
[30] M. G. Silveirinha, IEEE Trans. Antennas Propag. **54**, 1766 (2006).
[31] M. G. Silveirinha, C. A. Fernandes, and J. R. Costa, N. J. Phys. **10**, 053011 (2008).
[32] CST MICROWAVE STUDIO, CST GmbH, 2008 (www.cst.com).
[33] A. R. Melnyk and M. J. Harrison, Phys. Rev. B **2**, 835 (1970).
[34] M. Anderegg, B. Feuerbacher, and B. Fitton, Phys. Rev. Lett. **27**, 1565 (1971).
[35] M. G. Silveirinha and C. A. Fernandes, Phys. Rev. B **78**, 033108 (2008).